



HAL
open science

Sources and Sinks of Interannual Steric Sea Level Variability

Antoine Hochet, William Llovel, Florian Sévellec, Thierry Huck

► **To cite this version:**

Antoine Hochet, William Llovel, Florian Sévellec, Thierry Huck. Sources and Sinks of Interannual Steric Sea Level Variability. *Journal of Geophysical Research. Oceans*, 2023, 128 (4), pp.e2022JC019335. 10.1029/2022JC019335 . hal-04234389

HAL Id: hal-04234389

<https://hal.science/hal-04234389>

Submitted on 10 Oct 2023

HAL is a multi-disciplinary open access archive for the deposit and dissemination of scientific research documents, whether they are published or not. The documents may come from teaching and research institutions in France or abroad, or from public or private research centers.

L'archive ouverte pluridisciplinaire **HAL**, est destinée au dépôt et à la diffusion de documents scientifiques de niveau recherche, publiés ou non, émanant des établissements d'enseignement et de recherche français ou étrangers, des laboratoires publics ou privés.

Sources and sinks of interannual steric sea level variability

Antoine Hochet¹, William Llovel¹, Florian Sévellec¹, Thierry Huck¹

¹Laboratoire d'Océanographie Physique et Spatiale, CNRS, University of Brest, IFREMER, IRD, 29238 Plouzané, France

Key Points:

- The main source of interannual steric sea level variance is the advection of the mean density by interannual velocity anomalies.
- This source of variance is balanced by fluctuating net heat flux from the atmosphere and by the fluctuating eddy induced velocities.
- The main source of interannual steric sea level variance is mostly sustained by the wind variability via Ekman velocities.

Corresponding author: Antoine Hochet, ahochet@ifremer.fr

Abstract

Understanding the mechanisms of regional steric sea level variability is fundamental to understand the regional sea level variability recorded by satellite altimetry for years and to insure that future projections made by climate models are realistic. Here, we first develop a novel method based on steric sea level variance budget that allows to detect the sources and sinks of the variability. Using the “Estimating the Circulation and Climate of the Ocean” (ECCO V4) state estimate, we then show that interannual steric sea level variability is mainly sustained by interannual fluctuating winds via Ekman transport almost everywhere. The damping of the variability is made by both the interannual fluctuating net heat flux from the atmosphere, that largely dominates the atmospheric freshwater fluxes, and the parametrized effect of eddies. It is also found that the parametrized effect of diffusion on the variability is weak in most regions and that, although globally weak, the fluctuations of atmospheric freshwater fluxes are a source of variance close to the Equator in the Pacific ocean.

Plain Language Summary

Since the launch of Topex/Poseidon satellite in August 1992, sea level is routinely measured every ~ 10 days at a nearly global coverage. For the first time, satellite altimetry data show that regional sea level trends experience large regional variability compared to its global mean trend. If global mean sea level rise is a direct consequence of the on-going climate change, regional sea level change is more relevant for coastal impacts. Thus, investigating the regional sea level changes and its causes are of great importance for potential socio-economic impacts as 10% of the world’s population live at less than 10 meters above sea level. Those investigations are also important for assessing the reliability of coupled climate models used to predict future sea level changes. In this study, we develop a novel method based on the steric sea level variance budget to rigorously estimate the sources and sinks of the interannual steric sea level variability so as to understand the physical processes at play. We find the main source of interannual steric sea level variance is the advection of the mean density by interannual velocity anomalies which are sustained by the wind variability via Ekman velocities.

1 Introduction

Sea level change is one of the most direct consequences of the on-going climate change and may have several socio-economical coastal implications (Nicholls & Cazenave, 2010). Sea level change has been routinely recorded, with a nearly global coverage, by satellite altimetry missions since the launch of Topex/Poseidon in 1992 and its successors (Jason-1/2/3, ENVISAT, ERS1/2, Saral/Altika, Cryosat-2, and more recently Sentinel6-MF, etc). These high-quality data have demonstrated that the global mean sea level experiences a linear rise of 3.3 mm yr^{-1} [since over the 1993-2015 period](#) (WCRP Global Sea Level Budget Group, 2018). The global mean sea level is a good indicator of global warming but regional changes are most relevant for socio-economic impacts as roughly 10% of the world’s population lived at less than 10 meters above sea level especially in low-lying coastal and deltaic regions (Durand et al., 2019; Neumann et al., 2015). For the first time, satellite altimetry data have revealed that sea level is not rising uniformly and presents large deviations from its global mean trend. Indeed, some regions experience a linear rise 3 times as large as the global mean sea level trend [for instance in the western Pacific ocean, in the Indian ocean, and in the south Atlantic ocean [for the 2005-2013 period](#); Cazenave and Llovel (2010); Llovel and Lee (2015)].

Superimposed to the long-term trends, regional sea level interannual variability can enhance or reduce regional sea level change. This interannual variability of sea level is driven by modes of climate variability such as El Nino Southern Oscillation, the North Atlantic Oscillation, and the Indian Ocean Dipole in the north Indian ocean (Llovel et

al., 2010). This interannual variability has a steric origin: it is due to variations of temperature and salinity affecting density, resulting from changes in surface wind stress and buoyancy fluxes (Stammer et al., 2013). Therefore, investigating the interannual variability of steric sea level and their mechanisms appears to be highly relevant for understanding processes at play in regional sea level interannual variability. Moreover, understanding the interannual variability of regional sea level is essential to interpret satellite-based sea level observations relevant to ocean climate and to assess the reliability of future sea level projections made by coupled climate models.

Physical processes contributing to interannual variability of regional steric sea level have been studied using an observationally-constrained ocean state estimate produced by the “Estimating the Circulation and Climate of the Ocean” (ECCO) consortium (Piecuch & Ponte, 2011; Meyssignac et al., 2017). Piecuch and Ponte (2011) investigated the tendency changes of the vertically-integrated sea water density (i.e., steric sea level) due to fluctuating potential temperature and salinity. The tendencies of both tracers (potential temperature and salinity) are investigated by considering the conservation equation representing the effects of ocean advection, diffusion, and surface exchanges. This study suggested that the oceanic transports are more important than the surface buoyancy fluxes in setting the interannual variations of the steric sea level and that diffusion plays an important role at extratropical latitudes. This method has been widely used for identifying the physical processes at play in steric sea level interannual variability. However, this method presents some limitations as we cannot assess if the physical processes at play create or reduce the interannual steric sea level variability, in other words, if the physical process is a source or a sink of the interannual steric sea level variability.

Here we develop a novel method, based on the budget of the interannual steric sea level variance, to rigorously compute its sources and sinks and better understand its mechanisms. For this purpose, we use the ECCO V4 state estimate (Forget et al., 2015). The steric sea level variance budget is inspired from budget of density variance that were originally used to study the drivers of a multidecadal mode of variability in idealised simulations of the North Atlantic (Colin de Verdière & Huck, 1999; Arzel et al., 2006), in realistic configuration of the North Atlantic (Arzel et al., 2018; Gastineau et al., 2018), and mooring observations (Sévellec et al., 2021). Temperature variance budget have also been used in Hochet et al. (2020) to show that the non-linear transfer of temperature variance is directed from low to high frequencies. Here we transpose and adapt this approach to diagnose and partition as sources and sinks physical processes (advection, diffusion, and surface forcing) at play in the interannual steric sea level variability.

The remainder of this article is organized as follows: in section 2 we describe the method to obtain the steric sea level interannual variance budget. In section 3, we present the ECCO V4r3 state estimate. In section 4, the different terms of the steric sea level variance budget in the ECCO V4r3 state estimate are obtained. In section 5 we show how the steric sea level budget is related to the the more classical density variance budget already used in numerous previous studies. In section 6, we summarize and discuss the main conclusions of our study.

2 Method: steric sea level variance budget

Based on the hydrostatic and Boussinesq approximations, the barometrically-corrected sea level can be partitioned into local density change (due to change in temperature and salinity; this term is known as steric sea level) and local/regional mass change [known as manometric sea level, see Gregory et al. (2019) for more details on these terminologies].

$$\eta = \eta_{\text{steric}} + \eta_{\text{manometric}} = -\frac{1}{\rho_s} \int_{-H}^0 \rho \, dz + \frac{P_b}{\rho_0 g}, \quad (1)$$

111 where g is the acceleration due to gravity, H is the total ocean depth, ρ_s is a time and
 112 spatially constant representative surface density, ρ is the in situ density, and P_b is the
 113 ocean bottom pressure (Gill & Niiler, 1973). We use $\rho_s = \rho_0 = 1029 \text{ kg m}^{-3}$ in the
 114 remainder of this paper. Although manometric sea level variations are locally important
 115 at high latitudes, steric sea level variations are the main cause of interannual sea level
 116 variability in most regions (Lombard et al., 2005; Piecuch & Ponte, 2011; Carret et al.,
 117 2021) and is therefore the focus of this work. In what follows, we thus only consider the
 118 variations of η_{steric} .

119 The first step in computing the interannual steric sea level variance budget is to
 120 decompose every variable X into a time mean, an interannual component, and a high-
 121 frequency component:

$$X = \bar{X} + X^{\text{inter}} + X^{\text{HF}}, \quad (2)$$

122 where X is any time-dependent variable, \bar{X} represents the time mean of X over the con-
 123 sidered period of time, X^{inter} the interannual component of X which contains all frequen-
 124 cies strictly lower than the seasonal cycle, and X^{HF} the remaining high-frequency com-
 125 ponent of X which contains all the resolved frequency higher than annual including the
 126 seasonal cycle. The time derivative of the steric sea level equation gives the local evo-
 127 lution equation of its variations:

$$\frac{\partial \eta_{\text{steric}}^{\text{inter}}}{\partial t} = -\frac{1}{\rho_0} \int_{-H}^0 \frac{\partial \rho^{\text{inter}}}{\partial t} dz, \quad (3)$$

128 where t is time. As mentioned in the introduction, the main novelty of this work is to
 129 compute the local variance budget of the steric sea level. Because we are interested in
 130 the mean sources and sinks over the considered period of time, the budget is obtained
 131 as the time average of the product of the interannual steric sea level equation and its evo-
 132 lution from Eq. (3):

$$\overline{\eta_{\text{steric}}^{\text{inter}} \frac{\partial \eta_{\text{steric}}^{\text{inter}}}{\partial t}} = \frac{1}{2} \overline{\frac{\partial (\eta_{\text{steric}}^{\text{inter}})^2}{\partial t}} = \frac{1}{\rho_0^2} \int_{-H}^0 \overline{\rho^{\text{inter}} dz} \int_{-H}^0 \overline{\frac{\partial \rho^{\text{inter}}}{\partial t} dz}. \quad (4)$$

133 This demonstrates that this product is equal to the variations of the interannual steric
 134 sea level variance. To decompose the different terms of this budget, we thus need an evo-
 135 lution equation for ρ^{inter} . As in ECCO (Forget et al., 2015), we use the Jackett and Mc-
 136 dougall (1995) equation of state for density to link the density to the potential temper-
 137 ature θ and the salinity S and pressure:

$$\rho = \rho(S, \theta, -\rho_0 g z), \quad (5)$$

138 where the pressure is assumed to be a function of only depth (z). Then, the time deriva-
 139 tive of Eq. (5) gives the evolution equation for ρ as a function of θ and S :

$$\begin{aligned} \frac{\partial \rho}{\partial t} &= \rho_0 \left(-\alpha \frac{\partial \theta}{\partial t} + \beta \frac{\partial S}{\partial t} \right) \\ &= \underbrace{-\rho_0 \alpha \text{ADV}_{\theta} + \rho_0 \beta \text{ADV}_S}_{=\text{ADV}} \underbrace{-\rho_0 \alpha \text{DIF}_{\theta} + \rho_0 \beta \text{DIF}_S}_{=\text{DIF}} \underbrace{-\rho_0 \alpha \text{FLU}_{\theta} + \rho_0 \beta \text{FLU}_S}_{=\text{FLU}} \end{aligned} \quad (6)$$

140 where $\text{ADV}_{\theta,S}$, $\text{DIF}_{\theta,S}$ and $\text{FLU}_{\theta,S}$ represent respectively the θ , S advection, the param-
 141 eterized diffusion of temperature and salinity, and the net heat flux and freshwater fluxes
 142 from the atmosphere. [ECCO V4r3 provides all the necessary terms to close the tem-](#)
 143 [perature and salinity budgets. Temperature and salinity advection and diffusion are ob-](#)
 144 [tained from the divergence of the corresponding advective flux and diffusive flux which](#)

145 are direct outputs of the state estimate. Similarly, FLU_θ and FLU_S are also obtained
 146 from the direct outputs of ECCO V4r3. $\alpha = -1/\rho_0 \partial \rho / \partial \theta$ and $\beta = 1/\rho_0 \partial \rho / \partial S$ are respec-
 147 tively the thermal expansion and saline contraction coefficients obtained from the Jackett
 148 and McDougall (1995) equation of state for density. Note that the advection term regroups
 149 the resolved and parameterized eddy-induced transport; whereas the diffusion term re-
 150 groups the isopycnal, diapycnal and convective mixing collectively. Using Eq. (6), the
 151 equation for the interannual variations of density is thus:

$$\frac{\partial \rho^{\text{inter}}}{\partial t} = \text{ADV}^{\text{inter}} + \text{DIF}^{\text{inter}} + \text{FLU}^{\text{inter}}, \quad (7)$$

152 where $\text{ADV}^{\text{inter}}$ represents, the effect of advective terms, $\text{DIF}^{\text{inter}}$ the effect of diffusive
 153 terms, and $\text{FLU}^{\text{inter}}$ the buoyancy forcing from the atmosphere. Then, inserting Eq. (7)
 154 in Eq. (4) allows us to separate the steric sea level variance budget into advective, dif-
 155 fusive, and atmospheric fluxes contributions:

$$\frac{1}{2} \overline{\frac{\partial (\eta_{\text{steric}}^{\text{inter}})^2}{\partial t}} = \overline{\text{ADV}_{\text{steric}}} + \overline{\text{DIF}_{\text{steric}}} + \overline{\text{FLU}_{\text{steric}}} \quad (8)$$

156 where:

$$\overline{Y}_{\text{steric}} = \frac{1}{\rho_0^2} \overline{\int_{-H}^0 \rho^{\text{inter}} dz \int_{-H}^0 Y dz} \quad (9)$$

157 Y represents either $\text{ADV}^{\text{inter}}$, $\text{DIF}^{\text{inter}}$ or $\text{FLU}^{\text{inter}}$. The main advantage of this method
 158 (variance budget) compared to the direct budget of η_{steric} is that it gives the local sources
 159 and sinks of the variability: if $\overline{Y}_{\text{steric}}$ is positive (negative) then it is a source (sink) of
 160 steric sea level variance because it acts to increase (decrease) $\eta_{\text{steric}}^{\text{inter}}$ variance. Eq. (9) can
 161 also be written as:

$$\overline{Y}_{\text{steric}} = \overline{\eta_{\text{steric}}^{\text{inter}} B} \quad (10)$$

162 where $B = \frac{-1}{\rho_0} \int_{-H}^0 Y dz$. It is then apparent that $\overline{Y}_{\text{steric}}$ can be a source in two dif-
 163 ferent cases: 1) $\eta_{\text{steric}}^{\text{inter}}$ is positive and B is positive or 2) $\eta_{\text{steric}}^{\text{inter}}$ is negative and B is neg-
 164 ative. It is also interesting to note that it is the correlation between the vertical integral
 165 of the density anomaly and the vertical integral of the interannual anomaly of advec-
 166 tion, diffusion, or buoyancy surface flux that creates a sink or a source of steric sea
 167 level variance. Therefore, in Eq. (9) ρ^{inter} and Y do not need to be correlated at the
 168 same depths to create a source or a sink.

169 The results of the steric sea level variance budget applied to ECCO V4r3 outputs,
 170 as given by equation (8) will first be shown in section 4.1. Then the advective term of
 171 the budget ($\overline{\text{ADV}_{\text{steric}}}$) will be further decomposed into four different terms in section
 172 4.2.

173 3 Model

174 We assess the steric sea level variance budget using the ECCO V4r3 state estimate
 175 that covers the 1992-2017 period. This reanalysis is the output of the Massachusetts In-
 176 stitute of Technology general circulation model (MITgcm) assimilating available obser-
 177 vations for the period 1992 to 2017 (Forget et al., 2015). The advantage of this reanal-
 178 ysis is that it satisfies the equation of motion and conservation laws hence making it pos-
 179 sible to compute tracers budget. The solution used in this article is computed on the LLC90
 180 grid which has an average horizontal resolution of 1° and 50 vertical levels. Outputs of
 181 the model consist of one month average and the closed budget can be obtained for the

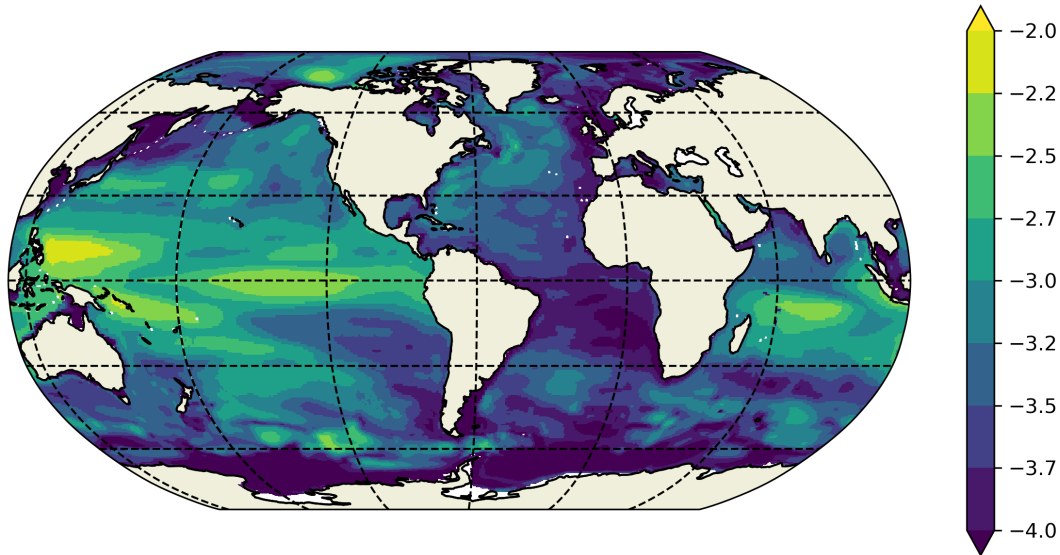


Figure 1. Time-variance of the interannual steric sea level (log scale, in m^2) obtained from the ECCO V4r3 state estimate and averaged over the period 1993-2014.

182 1993-2014 period. Thus we compute the steric sea level budget over this 1993-2014 pe-
 183 riod.

184 Interannual anomalies are computed by removing the time mean seasonal cycle from
 185 the monthly time series, then the subannual signal is removed using a Lanczos low-pass
 186 filter with a 1 year cutoff frequency. The interannual variability defined here thus con-
 187 tains all periods longer than 13 months (including the regional long-term steric sea level
 188 trends).

189 The interannual steric sea level variance computed from the ECCO V4r3 estimate
 190 (Figure 1) shows, in agreement with previous studies (Piecuch & Ponte, 2011, for instance),
 191 the largest values at low latitudes in the equatorial Pacific and in the Indian ocean. At
 192 high latitudes, it is interesting to note that large interannual variability of the steric sea
 193 level are found in the Beaufort gyre of the Arctic ocean. Fukumori et al. (2021) have shown
 194 that interannual variations in halosteric sea level in this region are linked with wind driven
 195 Ekman transport.

196 4 Interannual steric sea level variance budget

197 In this section, we first present the decomposition of the interannual steric sea level
 198 variance budget as given by Eq. (8), then show/derive the decomposition of the advective
 199 term and finally associate the advective source term with Ekman velocities.

200 4.1 Interannual steric sea level variance budget

201 The interannual steric sea level variance budget indicates the relative importance
 202 of the different terms (Figure 2). \overline{ADV}_{steric} is positive almost everywhere except in some
 203 localized regions of the western north Pacific low latitudes. The largest magnitudes are
 204 found in the eastern equatorial regions of the Pacific and Indian ocean. On the contrary,
 205 \overline{FLU}_{steric} is negative and compensates \overline{ADV}_{steric} almost exactly. Table 1 gives the global
 206 integral of the different terms of the interannual steric sea level variance budget. As ex-
 207 pected from the maps, the largest source is the advection (\overline{ADV}_{steric}) with $4.8 \times 10^{-12} \text{ m}^2 \text{ s}^{-1}$

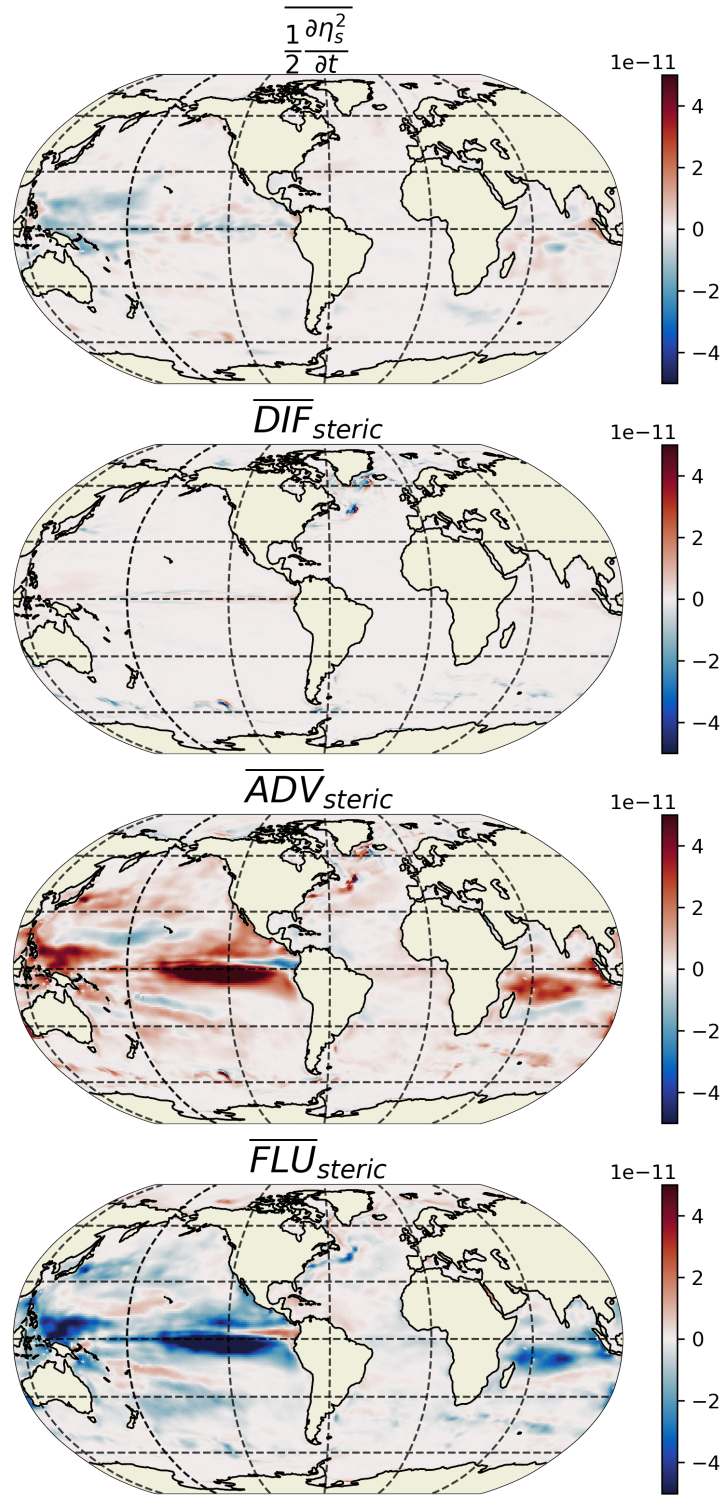


Figure 2. Terms of the interannual steric sea level variance budget (in $\text{m}^2 \text{s}^{-1}$) for total (top), diffusion (second line), advection (third line), and atmospheric fluxes (last line). The spatial integral obtained for each terms is given in table 1.

Table 1. Globally-averaged terms shown on figures 2, 3, and 4

Term	$10^{-12} \text{ m}^2 \text{ s}^{-1}$
Figures 2 and 3: $(\eta_s^{\text{inter}})^2$ budget	
$\frac{1}{2} \overline{\frac{\partial(\eta_s^{\text{inter}})^2}{\partial t}}$	-0.4
$\overline{\text{DIF}}_{\text{steric}}$	-0.2
$\overline{\text{ADV}}_{\text{steric}}$	4.8
$\overline{\text{FLU}}_{\text{steric}}$	-5.0
$\overline{\text{FLU}}_{\text{steric}}^{\text{THETA}}$	-5.7
$\overline{\text{FLU}}_{\text{steric}}^{\text{SALT}}$	0.7
Figure 4: advection decomposition	
$\overline{\text{ADV}}_{\text{steric}}^1$	13.8
$\overline{\text{ADV}}_{\text{steric}}^2$	-1.4
$\overline{\text{ADV}}_{\text{steric}}^3$	1.1
$\overline{\text{ADV}}_{\text{steric}}^4$	-8.7

208 and the largest sink is the atmospheric buoyancy flux ($\overline{\text{FLU}}_{\text{steric}}$) with $-5 \times 10^{-12} \text{ m}^2 \text{ s}^{-1}$.
209 The damping of steric sea level variations by atmospheric buoyancy flux is mainly as-
210 sociated with the interannual variations of the net heat flux (see figure 3 and table 1)
211 but variations of freshwater fluxes play a non-negligible role close to the equator in the
212 Pacific ocean (acting as a source of variance). The net interannual atmospheric heat flux
213 thus act to decrease the temperature when temperature anomalies are positive and to
214 increase the temperature when temperature anomalies are negative. Overall, the main
215 balance is therefore between the advection, which is a source of variance in almost all
216 regions and the net atmospheric heat flux which is a sink of variance. This is one of the
217 main results of this study which we believe has never been shown before. The amplitude
218 of these two terms is almost one order of magnitude larger than the amplitude of the pa-
219 rameterized diffusive term ($\overline{\text{DIF}}_{\text{steric}}$) and the time mean of the squared steric sea level
220 anomaly tendency ($\overline{\frac{\partial(\eta_s^{\text{inter}})^2}{\partial t}}$) (Fig. 2). The strongest magnitude of the time mean squared
221 steric sea level anomaly is found at low latitudes in the western Pacific and has nega-
222 tive values. These negative values are due to the decrease of the interannual variability
223 over the ECCO V4r3 period (1993-2014). The term $\overline{\frac{\partial(\eta_s^{\text{inter}})^2}{\partial t}}$ would be zero in a stable
224 climate (i.e. with a constant external forcing) and a time period sufficiently long to sam-
225 ple all the internal variability. Here, these two conditions are not satisfied: the climate
226 is not stable because of anthropogenic climate change and the 22 years period (1993-2014)
227 is too short to capture all the internal variability. The decrease of $\overline{\frac{\partial(\eta_s^{\text{inter}})^2}{\partial t}}$ in the west-
228 ern Pacific could therefore either be associated with anthropogenic climate change or with
229 decadal natural variability, but this question is outside the scope of this article. The dif-
230 fusion term ($\overline{\text{DIF}}_{\text{steric}}$) is at least one order of magnitude smaller than the advective and
231 atmospheric buoyancy flux terms and is weakly negative when integrated horizontally
232 (Table 1).

233 Several authors (Lombard et al., 2005; Llovel et al., 2010) have shown that the in-
234 terannual steric sea level variations in the Equatorial Pacific are associated with the El
235 Niño-Southern Oscillation (ENSO). In the Indian ocean, the interannual variations of
236 the steric sea level have been shown to be associated with the Indian Ocean Dipole (IOD)
237 (Llovel et al., 2010). Here we thus show that the main balance of the ENSO and IOD
238 associated steric sea level variations is the forcing made by the advective term and the
239 damping made by variations of net atmospheric heat flux.

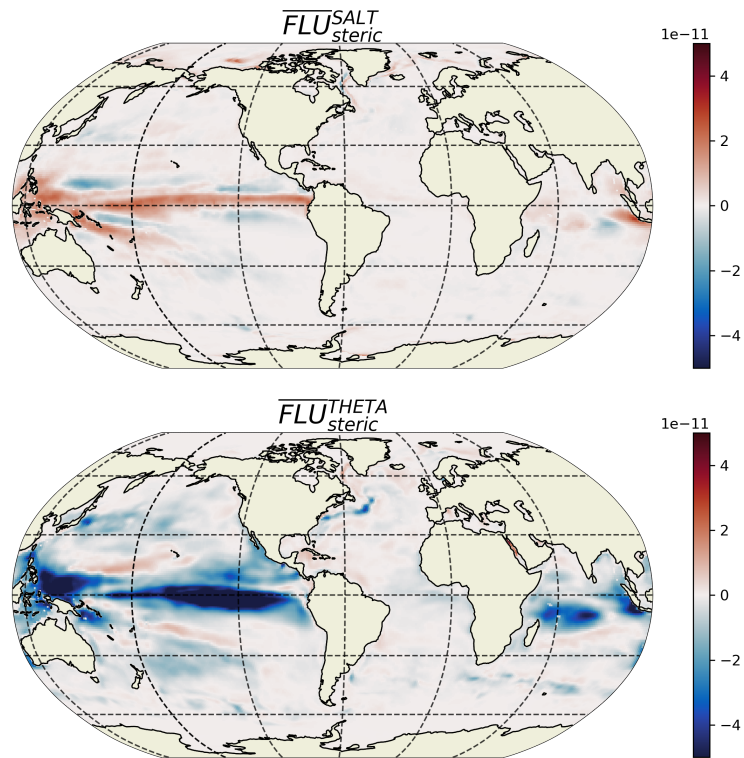


Figure 3. Decomposition of the atmospheric fluxes term ($\overline{FLU_{steric}}$, in m s^{-2}) into a part associated with salinity due freshwater fluxes (top panel) and a part associated with temperature and due to the net heat flux from the atmosphere (bottom panel). The spatial integral of the 2 terms is given in table 1.

240

4.2 Decomposition of the advective term

241

242

243

The advection term ADV can be expressed as a function of in-situ density by computing the product of the 3D velocity \mathbf{v} and the gradient of the equation of state for density (5):

$$\text{ADV} = -\rho_0 (-\alpha \nabla \cdot \mathbf{v} \theta + \beta \nabla \cdot \mathbf{v} S) = -\nabla \cdot \mathbf{v} \rho_{\text{in situ}} - wg \gamma \rho_0 \quad (11)$$

244

245

246

247

where $\gamma = 1/\rho_0 \partial \rho / \partial p$ is the pressure expansion coefficient. Thus ADV represents the advection of in-situ density plus a term due to its pressure dependence. Assuming that γ is a constant, we can define a depth-dependent background density $\rho_B(z)$ that satisfies $\frac{\partial \rho_B}{\partial z} = \gamma g \rho_0$. Then, writing $\rho^* = \rho_{\text{in situ}} + \rho_B(z)$, we have:

$$\text{ADV} = -\nabla \cdot \mathbf{v} \rho^* \quad (12)$$

248

249

250

251

252

which shows that ADV can be interpreted as the advection of the in-situ density corrected from its pressure dependence i.e. ρ^* . For the sake of conciseness, we drop the * superscript in what follows. Note that in practise, all terms in the following density advection decomposition are computed from the decomposition of the temperature and salinity advection given by the first equality in equation (11).

253

254

Using the timescale decomposition [Eq. (2)] from section 2, the interannual advective term that appears in Eq. (8) can be decomposed as:

$$\text{ADV}^{\text{inter}} = -\nabla \cdot (\mathbf{v} \rho)^{\text{inter}} = \underbrace{-\nabla \cdot \mathbf{v}^{\text{inter}} \bar{\rho}}_{=\text{adv}_1} - \underbrace{\nabla \cdot \bar{\mathbf{v}} \rho^{\text{inter}}}_{=\text{adv}_2} - \underbrace{\nabla \cdot \mathbf{v}^{\text{inter}} \rho^{\text{inter}}}_{=\text{adv}_3} + \underbrace{R^{\text{HF}}}_{=\text{adv}_4}, \quad (13)$$

255

256

257

258

259

260

261

262

263

where adv_1 is the advection of mean density by interannual anomalous velocities, adv_2 is the advection of interannual density by mean velocities, adv_3 is the non-linear self advection of interannual density and adv_4 is the residual, containing the rectification effect of higher frequencies due to the correlation of submonthly velocity and submonthly density anomalies and the effect of Gent and McWilliams parameterized eddies (Gent & McWilliams, 1990, GM hereafter). (The expression for adv_4 is given in Appendix A for reference but is computed as a residual in practice.) Using Eq. (13), the advective term of the steric sea level variance budget [see Eq. (8)] can thus be decomposed into four terms as:

$$\overline{\text{ADV}}_{\text{steric}} = \sum_{i=1}^4 -\frac{\overline{\eta^{\text{inter}}}}{\rho_0} \int_{-H}^0 \overline{\text{adv}_i} dz = \sum_{i=1}^4 \overline{\text{ADV}}_{\text{steric}}^i \quad (14)$$

264

265

266

267

268

269

270

271

272

273

274

275

276

277

where the notation $\overline{\text{ADV}}_{\text{steric}}^i$ is given by formula (9) with $Y = \text{adv}_i$. The four terms from the decomposition of the $\overline{\text{ADV}}_{\text{steric}}$ term are shown in Figure 4. In most of the regions, the advection of mean density by interannual velocity is positive although it can be negative in some localized regions (e.g. in the eastern Equatorial Pacific). Globally, it is the largest source of steric sea level variance (Fig. 4 top left panel) with a horizontal average of $13.8 \times 10^{-12} \text{ m}^2 \text{ s}^{-1}$. Locally this source term is balanced by both the advection of ρ^{inter} by mean velocities and by the HF rectification term. However, globally, the spatial integral of the two terms reveals that the main sink is the HF rectification term (horizontal average: $-8.7 \times 10^{-12} \text{ m}^2 \text{ s}^{-1}$). Indeed, an important compensation occurs between the spatial integral of $\overline{\text{ADV}}_{\text{steric}}^1$ (source term) and the spatial integral of the rectification effect of higher frequencies (sink term). This HF rectification term is mostly the result of the GM parameterization of eddy induced velocities (not shown). Remarkably, the compensation between the source $\overline{\text{ADV}}_{\text{steric}}^1$ and the sink term due to the GM parameterization of eddies is locally important in the Beaufort gyre in the Arctic ocean

278 where their sum almost cancel out. The term linked with the advection of interannual
 279 density anomalies by mean velocities, i.e. $\overline{\text{ADV}_{\text{steric}}^2}$, is an important local sink of inter-
 280 annual steric sea level variance mainly in the western equatorial Pacific, it can also be
 281 a source in the equatorial eastern Pacific and western Indian ocean. When horizontally
 282 integrated $\overline{\text{ADV}_{\text{steric}}^2}$ is weakly negative. The term linked with the non-linear self advec-
 283 tion of interannual density ($\overline{\text{ADV}_{\text{steric}}^3}$) is, in most regions, negligible except at low lat-
 284 itudes where it is generally positive. Globally, the two main terms composing the ad-
 285 vection part of the interannual steric sea level budget are thus: 1) a source term made
 286 by the advection of mean density by interannual velocities and 2) a sink term, mainly
 287 due to the GM parameterization of eddy velocities.

288 4.3 Role of Ekman velocities in interannual steric sea level variability

289 In this subsection, we show that $\overline{\text{ADV}_{\text{steric}}^1}$ can be explained by the direct effect of
 290 wind via Ekman velocities. To this end, we compute the term of the steric sea level vari-
 291 ance budget that corresponds to the transport of mean density by interannual Ekman
 292 velocities:

$$\text{ADV}^{\text{Ekman}} = \frac{\eta^{\text{inter}}}{\rho_0} \int_{-D_{\text{ek}}}^0 \nabla \cdot \mathbf{v}_{\text{Ekman}}^{\text{inter}} \bar{\rho} dz \quad (15)$$

293 where $\mathbf{v}_{\text{Ekman}}^{\text{inter}}$ is the 3D interannual Ekman velocity in the Ekman layer whose depth D_{ek}
 294 is assumed everywhere constant. We assume that the horizontal Ekman velocities are
 295 0 below the Ekman layer (i.e. $z < D_{\text{ek}}$) and depth independent in the Ekman layer (for
 296 $0 > z > D_{\text{ek}}$) and given by:

$$(u_{\text{ek}}^{\text{inter}}, v_{\text{ek}}^{\text{inter}}) = \frac{1}{D_{\text{ek}} f_0 \rho_0} (\tau_y^{\text{inter}}, -\tau_x^{\text{inter}}) \quad (16)$$

297 where f_0 is the Coriolis parameter and (τ_x, τ_y) ($\tau_x^{\text{inter}}, \tau_y^{\text{inter}}$) are the zonal and meridional
 298 components of the interannual anomalies of momentum stress due to wind. Note that
 299 the momentum stress takes into account the effect of sea-ice at high latitudes. The ver-
 300 tical Ekman velocity in the Ekman layer is then obtained from the vertical integral of
 301 the continuity equation as:

$$w_{\text{ek}}^{\text{inter}}(z) = -z \left(\frac{\partial u_{\text{ek}}^{\text{inter}}}{\partial x} + \frac{\partial v_{\text{ek}}^{\text{inter}}}{\partial y} \right) \quad (17)$$

302 $(u_{\text{ek}}^{\text{inter}}, v_{\text{ek}}^{\text{inter}}, w_{\text{ek}}^{\text{inter}}) \mathbf{v}_{\text{Ekman}}^{\text{inter}} = (u_{\text{ek}}^{\text{inter}}, v_{\text{ek}}^{\text{inter}}, w_{\text{ek}}^{\text{inter}})$ is then used to compute $\text{ADV}^{\text{Ekman}}$ from
 303 equation (15). We choose to use $D_{\text{ek}} = 50$ m. Because the Ekman velocities are inversely
 304 proportional to D_{ek} and are vertically integrated over D_{ek} , we find that $\text{ADV}^{\text{Ekman}}$ is
 305 almost independent of the choice of D_{ek} (tested values: D_{ek} between 20 m and 100 m)
 306 as already noticed by Buckley et al. (2014) for the variation of temperature in the mixed
 307 layer due to Ekman velocities. $\text{ADV}^{\text{Ekman}}$ is shown in the top panel of figure 5. Values
 308 are positive in most of the region and the largest magnitudes are found at low latitudes
 309 in qualitative agreement with $\overline{\text{ADV}_{\text{steric}}^1}$ (top panel, Figure 4). Positive values of $\text{ADV}^{\text{Ekman}}$
 310 are also found in the Beaufort gyre in the Arctic ocean, suggesting that the surface mo-
 311 mentum stress is an important source of interannual steric sea level variance in this re-
 312 gion. The fact that $\text{ADV}^{\text{Ekman}}$ is qualitatively similar to $\overline{\text{ADV}_{\text{steric}}^1}$ suggests that $\overline{\text{ADV}_{\text{steric}}^1}$
 313 is mainly contained to the surface Ekman layer. This is confirmed by the vertical inte-
 314 gral in the Ekman layer of the term associated with adv_1 (top panel of figure 5) i.e.:

$$-\frac{\eta^{\text{inter}}}{\rho_0} \int_{-D_{\text{ek}}}^0 \text{adv}_1 dz \quad (18)$$

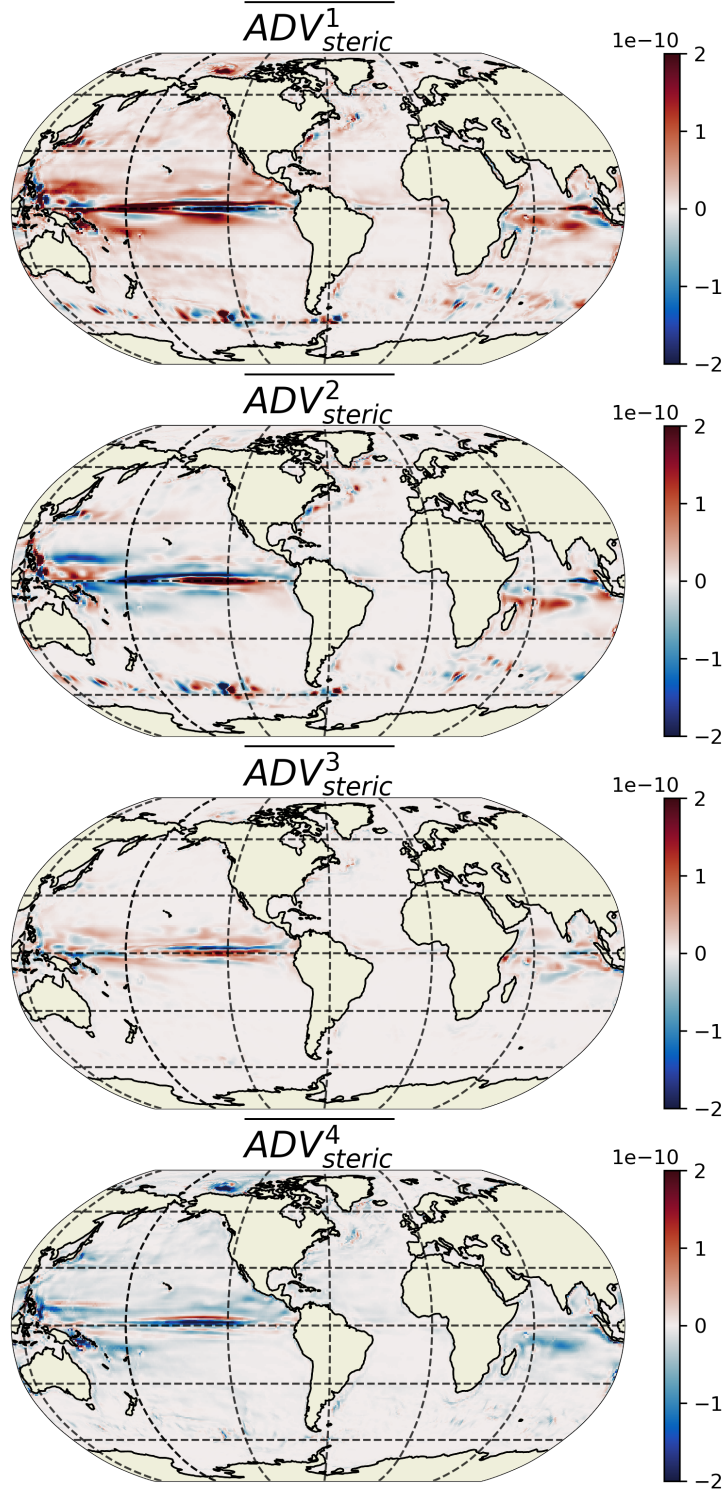


Figure 4. Decomposition of the advective term of the interannual steric sea level variability budget (in $\text{m}^2 \text{s}^{-1}$) into: the advection of mean density by interannual velocity ($\overline{\text{ADV}}^1_{\text{steric}}$, top), the advection of interannual density by mean velocity ($\overline{\text{ADV}}^2_{\text{steric}}$, second row), the non-linear self advection of interannual density ($\overline{\text{ADV}}^3_{\text{steric}}$, third row), and the rectification effect of higher frequencies including the action of GM eddy-induced advection ($\overline{\text{ADV}}^4_{\text{steric}}$, bottom). The spatial integrals of the 4 terms are given in table 1. The sum of these 4 terms gives the total advection shown in Fig. 2, bottom left panel.

315 which is almost identical to $\overline{\text{ADV}_{\text{steric}}^1}$ (top panel, Figure 4). Note that we have also tested
 316 the reconstruction of $\overline{\text{ADV}_{\text{steric}}^2}$ using Ekman velocities, however, the agreement between
 317 the reconstruction and $\overline{\text{ADV}_{\text{steric}}^2}$ is low suggesting that other processes must be at play.
 318 This reconstruction is thus not shown.

319 In the Indian ocean, the main mode of interannual steric level variability is the In-
 320 dian Ocean Dipole (Llovel et al., 2010), this dipole is associated with large scale SST vari-
 321 ations forced by interannual wind variations (Saji et al., 1999). In agreement with this
 322 wind forced mode of variability, the interannual wind variations act as a source of steric
 323 sea level variability in the western part of the equatorial Indian basin. However, nega-
 324 tive values are found in the Eastern part, which suggests that, in this region, interan-
 325 nual wind variations may also act as a sink of interannual steric sea level variability. In-
 326 terestingly, the total effect of advection $\overline{\text{ADV}_{\text{steric}}}$ (see Figure 2) is always positive in the
 327 equatorial Indian region suggesting that the sink effect of wind variations is balanced by
 328 an advective source. Figure 4 reveals that both $\overline{\text{ADV}_{\text{steric}}^2}$ and $\overline{\text{ADV}_{\text{steric}}^3}$, respectively
 329 the advection made by the mean velocity and the self advection have positive values in
 330 this region and thus compensate the damping of interannual steric sea levels variabil-
 331 ity made by the wind.

332 5 Link between steric sea level variance budget and density variance 333 budget

334 In this section, we show that the steric sea level variance budget developed in the
 335 previous sections is proportional to the vertically integrated barotropic density variance
 336 budget. As will be explained below, the barotropic density variance budget is a compo-
 337 nent of the density variance budget which was used in many past studies (e.g., Colin de
 338 Verdière & Huck, 1999; Huck et al., 1999; Arzel et al., 2018; Gastineau et al., 2018) to
 339 understand the mechanisms of a multidecadal mode of variability in the North Atlantic.
 340 The use of the barotropic variance budget will allow us to interpret the different terms
 341 of the steric sea level variance budget as transfers of density variance between different
 342 density variance reservoirs. Additionally, density variance is close to the Quasi-Geostrophic
 343 (QG) Available Potential Energy (APE), indeed, interannual QG APE is associated to
 344 the interannual density variance through the following formula (see Vallis, 2017, for in-
 345 stance):

$$\text{APE}_{\text{QG}}^{\text{inter}} = \frac{1}{2} \frac{g^2 (\rho^{\text{inter}})^2}{\rho_0 N_s^2(z)}, \quad (19)$$

346 where $N_s^2(z)$ is the horizontally averaged Brunt Vaisala frequency. However, because $N_s^2(z)$
 347 is depth dependent, $\text{APE}_{\text{QG}}^{\text{inter}}$ is proportional to the vertically integrated density variance
 348 only where the $N_s^2(z)$ depth dependency is negligible.

349 5.1 Density variance decomposition

350 The interannual density anomaly can be decomposed into barotropic and baroclinic
 351 parts as:

$$\rho^{\text{inter}} = \rho_{\text{BT}}^{\text{inter}} + \rho_{\text{BC}}^{\text{inter}}, \quad (20)$$

352 where $\rho_{\text{BT}}^{\text{inter}}$ and $\rho_{\text{BC}}^{\text{inter}}$ are the barotropic and baroclinic parts of ρ^{inter} , respectively, with
 353 $\rho_{\text{BT}}^{\text{inter}}$ the vertically averaged density anomaly (i.e., $\rho_{\text{BT}}^{\text{inter}} = \frac{1}{H} \int_{-H}^0 \rho^{\text{inter}} dz$) and $\rho_{\text{BC}}^{\text{inter}} =$
 354 $\rho^{\text{inter}} - \rho_{\text{BT}}^{\text{inter}}$. Using the relationship between the density anomaly and the steric sea level
 355 given by Eq. (1), we have:

$$\rho_{\text{BT}}^{\text{inter}} = -\frac{\rho_0}{H} \eta^{\text{inter}}. \quad (21)$$

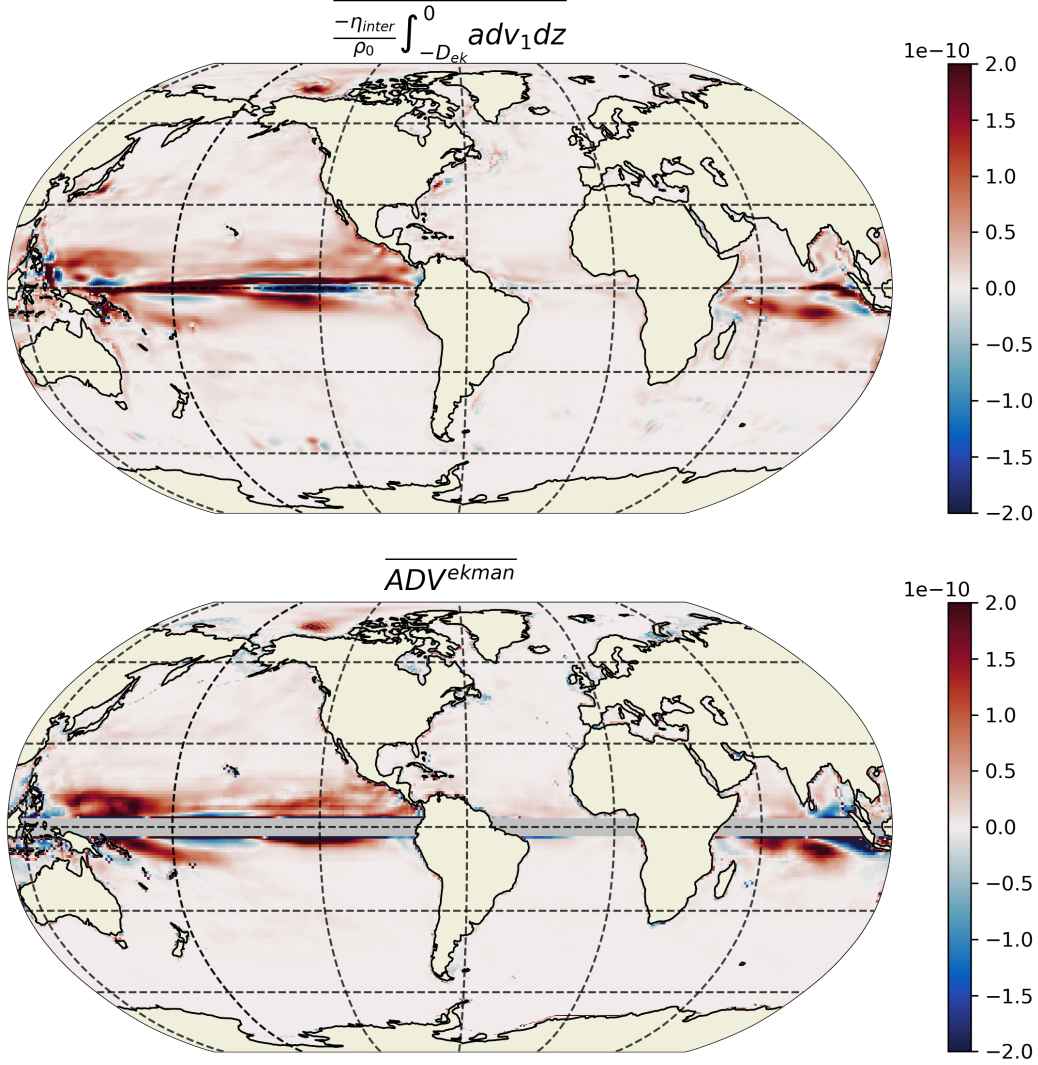


Figure 5. Top panel: same as $\overline{ADV_{steric}^1}$ (top panel, Figure 4) but where adv_1 is vertically integrated in the Ekman layer instead of over the full depth. Bottom panel: $\overline{ADV_{ekman}^{Ekman}}$ (in $m^2 s^{-1}$): term associated with the advection of the mean density by 3D Ekman velocities, vertically integrated in the Ekman layer [see formula Eq. (15)]. The grey band close to the equator corresponds to the region where the Ekman balance does not hold.

356 Thus, steric sea level anomalies can also be interpreted as barotropic density anomalies.
 357 It should be noted that because it is well established that the interannual steric sea level
 358 variations are mainly due to density anomalies close to the ocean surface (Willis et al.,
 359 2004; Llovel et al., 2013), the barotropic interannual density anomalies therefore also mainly
 360 reflect surface density anomalies. Using equation (2) to decompose the density ρ into dif-
 361 ferent timescales and the vertical decomposition of the interannual density anomaly (Eq. (20))
 362 gives:

$$\rho = \bar{\rho} + \rho_{\text{BT}}^{\text{inter}} + \rho_{\text{BC}}^{\text{inter}} + \rho^{\text{HF}}. \quad (22)$$

363 Using this decomposition, we show in Appendix B that the vertically integrated density
 364 variance is the sum of four terms:

$$\int_{-H}^0 \overline{\rho^2} dz = \int_{-H}^0 \overline{\bar{\rho}^2} dz + \int_{-H}^0 \overline{(\rho_{\text{BT}}^{\text{inter}})^2} dz + \int_{-H}^0 \overline{(\rho_{\text{BC}}^{\text{inter}})^2} dz + \int_{-H}^0 \overline{\rho_{\text{HF}}^2} dz. \quad (23)$$

The first term on the rhs is the vertically integrated squared mean density, the second
 and third terms, the vertically integrated interannual density variance, split between its
 barotropic and baroclinic parts and the last term the high-frequency density variance
 which contains all resolved sub annual frequencies. These four reservoirs are schemat-
 ically shown in Figure 6 as black boxes. The focus here is on all the transfers toward or
 from the barotropic density variance which is proportional to the steric sea level vari-
 ance. Indeed, using Eq. (21), it is easily seen that:

$$\overline{(\eta^{\text{inter}})^2} = \frac{H}{\rho_0^2} \int_{-H}^0 \overline{(\rho_{\text{BT}}^{\text{inter}})^2} dz. \quad (24)$$

365 Thus, the budget for the vertical integral of $(\rho_{\text{BT}}^{\text{inter}})^2$ is the same as the budget for the
 366 steric sea level variance, up to a factor $\frac{H}{\rho_0^2}$. Note that we add “unresolved eddies” to
 367 the high-frequency density variance reservoir in Figure 6 to be coherent with the trans-
 368 fer made by the parametrized GM eddy induced velocities, we thus implicitly assume that
 369 the parametrized eddies have subannual frequencies.

370 5.2 Equation for the evolution of the barotropic density variance

371 An equation for the evolution of the interannual barotropic density is obtained by
 372 vertically integrating the product of Eq. (7) and $\frac{1}{H}$:

$$\frac{\partial \rho_{\text{BT}}^{\text{inter}}}{\partial t} = \text{ADV}_{\text{BT}} + \text{DIF}_{\text{BT}} + \text{FLU}_{\text{BT}}, \quad (25)$$

373 where $X_{\text{BT}} = \frac{1}{H} \int_{-H}^0 X dz$ with X being ADV, DIF or FLU. Multiplying this equa-
 374 tion by $\rho_{\text{BT}}^{\text{inter}}$ and integrating vertically give the evolution equation for the vertically in-
 375 tegrated $\rho_{\text{BT}}^{\text{inter}}$ variance:

$$\int_{-H}^0 \frac{1}{2} \frac{\partial (\rho_{\text{BT}}^{\text{inter}})^2}{\partial t} dz = H \overline{\rho_{\text{BT}}^{\text{inter}} \text{ADV}_{\text{BT}}} + H \overline{\rho_{\text{BT}}^{\text{inter}} \text{DIF}_{\text{BT}}} + H \overline{\rho_{\text{BT}}^{\text{inter}} \text{FLU}_{\text{BT}}}. \quad (26)$$

376 The first term on the rhs is the effect of advection on the interannual barotropic den-
 377 sity variance and is represented by the sum of four blue arrows in Fig. 6 (the decom-
 378 position of this term will be explained below). The second and third terms respectively
 379 represent the effect of interannual barotropic diffusion (green arrow in Fig. 6) and interan-
 380 nual barotropic buoyancy flux from the atmosphere (red arrow in Fig. 6). Using the de-
 381 composition given by equation (13) in the advective term gives:

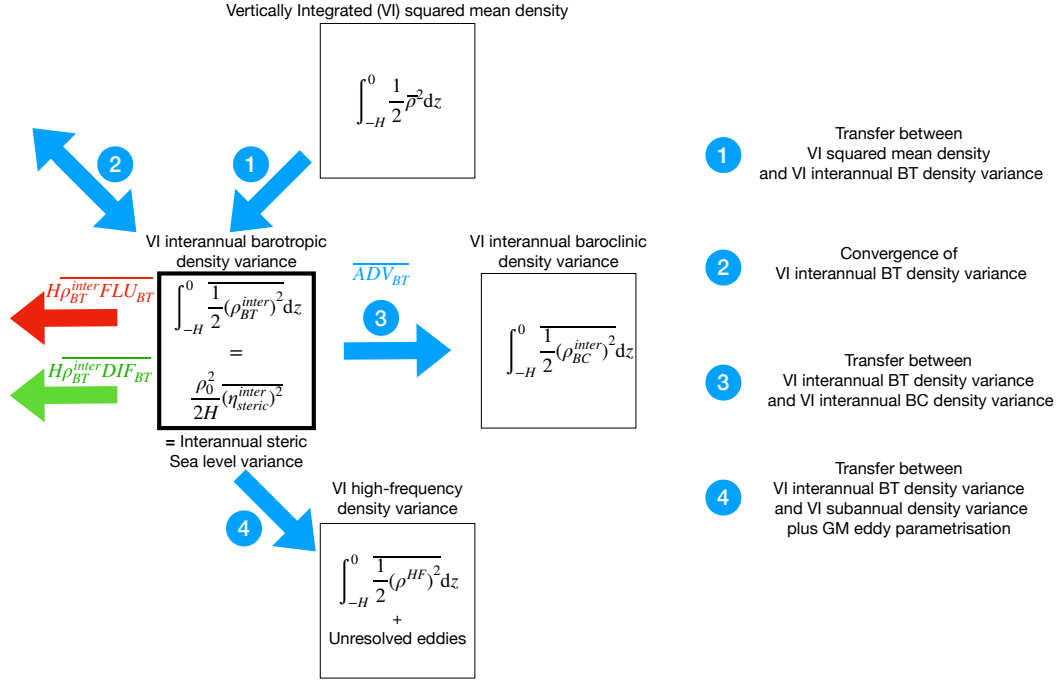


Figure 6. Schematic showing the four reservoirs under consideration here: the Vertically Integrated (VI) squared mean density (top box), the VI interannual barotropic (middle left) and baroclinic (middle right) density variance and the VI high-frequency density variance. The focus is on the interannual barotropic density variance (outlined by a thicker black box) because it is proportional to the interannual steric sea level variance. The red arrow represents the transfer of buoyancy from the atmosphere, the green arrow the diffusion effect and the blue arrows the effect of advection. Advection is decomposed into four terms 1,2,3 and 4 explained in the schematic. Note that because we attribute the term due to the GM parameterization of eddy induced velocities to the transfer between interannual and HF density variance, the HF density variance is assumed to also contains the unresolved eddies. The directions of the different arrows are chosen to represent the sign of each transfer when horizontally integrated over the total ocean area (see table 1). The transfer is a source (sink) when it is directed toward (from) the interannual barotropic density variance reservoir, the only exception is the interannual BT density variance convergence represented by blue arrow 2 which disappears when horizontally integrated.

$$H \overline{\rho_{\text{BT}}^{\text{inter}} \text{ADV}_{\text{BT}}} = \overline{\rho_{\text{BT}}^{\text{inter}} \int_{-H}^0 \text{adv}_1 dz} + \overline{\rho_{\text{BT}}^{\text{inter}} \left(\int_{-H}^0 (\text{adv}_2 + \text{adv}_3) dz \right)} + \overline{\rho_{\text{BT}}^{\text{inter}} \int_{-H}^0 \text{adv}_4 dz}. \quad (27)$$

382 We interpret below the different terms of this decomposition.

383 5.3 Transfer from the squared mean density

384 The product of $\int_{-H}^0 \text{adv}_1 dz$ and $\rho_{\text{BT}}^{\text{inter}}$ can be written as:

$$\overline{\rho_{\text{BT}}^{\text{inter}} \int_{-H}^0 \text{adv}_1 dz} = - \int_{-H}^0 \overline{\rho_{\text{BT}}^{\text{inter}} \mathbf{v}^{\text{inter}} \cdot \nabla \bar{\rho}} dz. \quad (28)$$

385 This term is interpreted as the transfer between the squared mean density reservoir and
 386 the interannual barotropic density variance reservoir. It is represented by a ~~black~~blue
 387 arrow number 1 between the vertically integrated squared mean density reservoir and the
 388 barotropic interannual density variance reservoirs in Fig. 6. This term has been stud-
 389 ied by many authors because it has been identified as a possible source of multidecadal
 390 North Atlantic variability (e.g., Colin de Verdière & Huck, 1999; Huck et al., 1999; Arzel
 391 et al., 2018; Gastineau et al., 2018). It is positive when the fluctuating transport of anoma-
 392 lous density ($\overline{\mathbf{v}^{\text{inter}} \rho_{\text{BT}}^{\text{inter}}}$) is directed downward the mean density gradient ($\nabla \bar{\rho}$) i.e. when
 393 $\overline{\mathbf{v}^{\text{inter}} \rho_{\text{BT}}^{\text{inter}} \cdot \nabla \bar{\rho}} < 0$. An intuitive interpretation is that, in this case, the fluctuating
 394 part acts to weaken the mean density gradient by transporting positive density anoma-
 395 lies toward low values of mean density and negative values toward high values of mean
 396 density.

397 5.4 Barotropic density variance convergence and transfer between barotropic 398 and baroclinic density variance

399 Using the vertical decomposition of the velocity and density into the advective term,
 400 first without any timescale decomposition gives:

$$-\nabla \cdot (\mathbf{v}\rho) = -\nabla \cdot (\mathbf{v}_{\text{BT}}\rho_{\text{BT}}) - \nabla \cdot (\mathbf{v}_{\text{BC}}\rho_{\text{BT}}) - \nabla \cdot (\mathbf{v}_{\text{BT}}\rho_{\text{BC}}) - \nabla \cdot (\mathbf{v}_{\text{BC}}\rho_{\text{BC}}). \quad (29)$$

401 The vertical integral of the terms involving only one BC term is zero and we are thus
 402 left with the following expression for the barotropic part of the advective term:

$$\frac{1}{H} \int_{-H}^0 -\nabla \cdot (\mathbf{v}\rho) dz = -\nabla \cdot (\mathbf{v}_{\text{BT}}\rho_{\text{BT}}) - \frac{1}{H} \int_{-H}^0 \nabla \cdot (\mathbf{v}_{\text{BC}}\rho_{\text{BC}}) dz. \quad (30)$$

403 Applying this vertical decomposition (30) to the sum of terms adv_3 and adv_4 from (13)
 404 gives (see details in Appendix C):

$$\overline{\rho_{\text{BT}}^{\text{inter}} \int_{-H}^0 (\text{adv}_3 + \text{adv}_4) dz} = -\nabla \cdot \left(\overline{\mathcal{V}_{\text{BT}} \frac{(\rho_{\text{BT}}^{\text{inter}})^2}{2}} \right) - \frac{1}{H} \int_{-H}^0 \overline{\rho_{\text{BT}}^{\text{inter}} \nabla \cdot (\mathcal{V}_{\text{BC}} \rho_{\text{BC}}^{\text{inter}})} dz \quad (31)$$

405 where $\mathcal{V}_{\text{BT}} = \overline{\mathbf{v}_{\text{BT}}} + \mathbf{v}_{\text{BT}}^{\text{inter}}$ and $\mathcal{V}_{\text{BC}} = \overline{\mathbf{v}_{\text{BC}}} + \mathbf{v}_{\text{BC}}^{\text{inter}}$. In this formula, the first term on
 406 the rhs is the convergence of the interannual barotropic density variance by the sum of
 407 the mean barotropic and interannual barotropic velocities. This term disappears when
 408 integrated horizontally and thus cannot be a global source or sink of interannual barotropic
 409 density variance, it is represented by blue arrow number 2 in Fig. 6. The last term in
 410 the rhs is the transfer between the interannual baroclinic and barotropic density vari-
 411 ance, it is represented by blue arrow number 3 in Fig. 6. The convergence and transfer

412 terms are plotted in Figure 7, the convergence of interannual barotropic density variance
 413 is almost everywhere smaller than the transfer between the barotropic and baroclinic in-
 414 terannual density variance. This is not surprising since the baroclinic part of the circu-
 415 lation is much larger than the barotropic part almost everywhere. This term is quali-
 416 tatively similar to $\overline{\text{ADV}_{\text{steric}}^2}$ (see Fig. 4), the term due to the advection of density anoma-
 417 lies by the time mean velocity, which dominates over $\overline{\text{ADV}_{\text{steric}}^3}$. It is mostly positive in
 418 the Indian ocean, indicating that the baroclinic/barotropic transfer is, in this region, a
 419 source of interannual steric sea level variance and have both sign in the equatorial Pa-
 420 cific ocean. Its spatial integral is equal to the sum of the spatial integral of terms $\overline{\text{ADV}_{\text{steric}}^2}$
 421 and $\overline{\text{ADV}_{\text{steric}}^3}$ and is thus weakly negative ($-0.3 \times 10^{-12} \text{ m}^2 \text{ s}^{-1}$). Note that in figure 7,
 422 the formula from Eq. (31) has been rescaled by H/ρ_0^2 to correspond to the steric sea level
 423 (following Eq. (24)) which is the focus of this article.

424 5.5 Transfer to HF density variance and GM parameterization of eddy 425 velocity

426 The last term is:

$$\rho_{\text{BT}}^{\text{inter}} \int_{-H}^0 \text{adv}_4 \, dz = \rho_{\text{BT}}^{\text{inter}} \int_{-H}^0 R_{\text{HF}} \, dz. \quad (32)$$

427 This term is a sink of barotropic variance (Fig. 6). The HF has already been identified
 428 in Hochet et al. (2020, 2022) as acting as a damping effect on the lower frequencies. This
 429 induces a density variance transfer from low to high frequencies, consistently with local
 430 observations near the Drake passage (Sévellec et al., 2021). High frequencies associated
 431 with smaller spatial scales tend to erode the large scale gradients associated with low fre-
 432 quencies. Because of the link between the density variance and the QG APE it can also
 433 be thought as a direct APE cascade in the temporal scale as explained in Arbic et al.
 434 (2014). As mentioned in last section, in ECCO V4r3, this transfer is dominated by the
 435 term linked with GM eddy induced velocities rather by the resolved subannual circula-
 436 tion. This transfer is represented by the blue arrow 4 in Fig. 6.

437 6 Conclusion and Discussion

438 In this article we have developed a new diagnostic based on interannual steric sea
 439 level variance budget that allows to robustly assess the sources and sinks of interannual
 440 steric sea level variability. Using the ECCO V4r3 state estimate, we have shown that in
 441 most regions, the main equilibrium is between the advection which is a source of steric
 442 sea level variance and the buoyancy flux from the atmosphere which is a sink of variance.
 443 The atmospheric buoyancy flux is largely dominated by the net heat flux exchange with
 444 the atmosphere. When horizontally integrated, the diffusive term is one order of mag-
 445 nitude smaller than the advection and the atmospheric buoyancy flux. The advective term
 446 can further be decomposed into four different terms which can be associated to differ-
 447 ent barotropic density variance transfers between different density variance reservoirs.
 448 The decomposition of the advection reveals that the main source of interannual variabil-
 449 ity is the self advection of interannual barotropic density anomalies in the direction op-
 450 posite to the mean density gradient. In this process, the interannual circulation extracts
 451 energy from the mean circulation by eroding the large scale mean density gradient. This
 452 term is interpreted as a transfer of barotropic density variance between the mean and
 453 the interannual density variance. The same term was previously found to be one of the
 454 possible source of the Atlantic multidecadal variability (e.g., Arzel et al., 2018, and ref-
 455 erences therein). It is then shown that the velocities associated with this transfer are mainly
 456 the result of interannual variations of the surface wind stress by means of the Ekman bal-
 457 ance. This source term is thus an intrinsic transfer of energy between two oceanic reser-
 458 voirs triggered by an atmospheric source of variability.

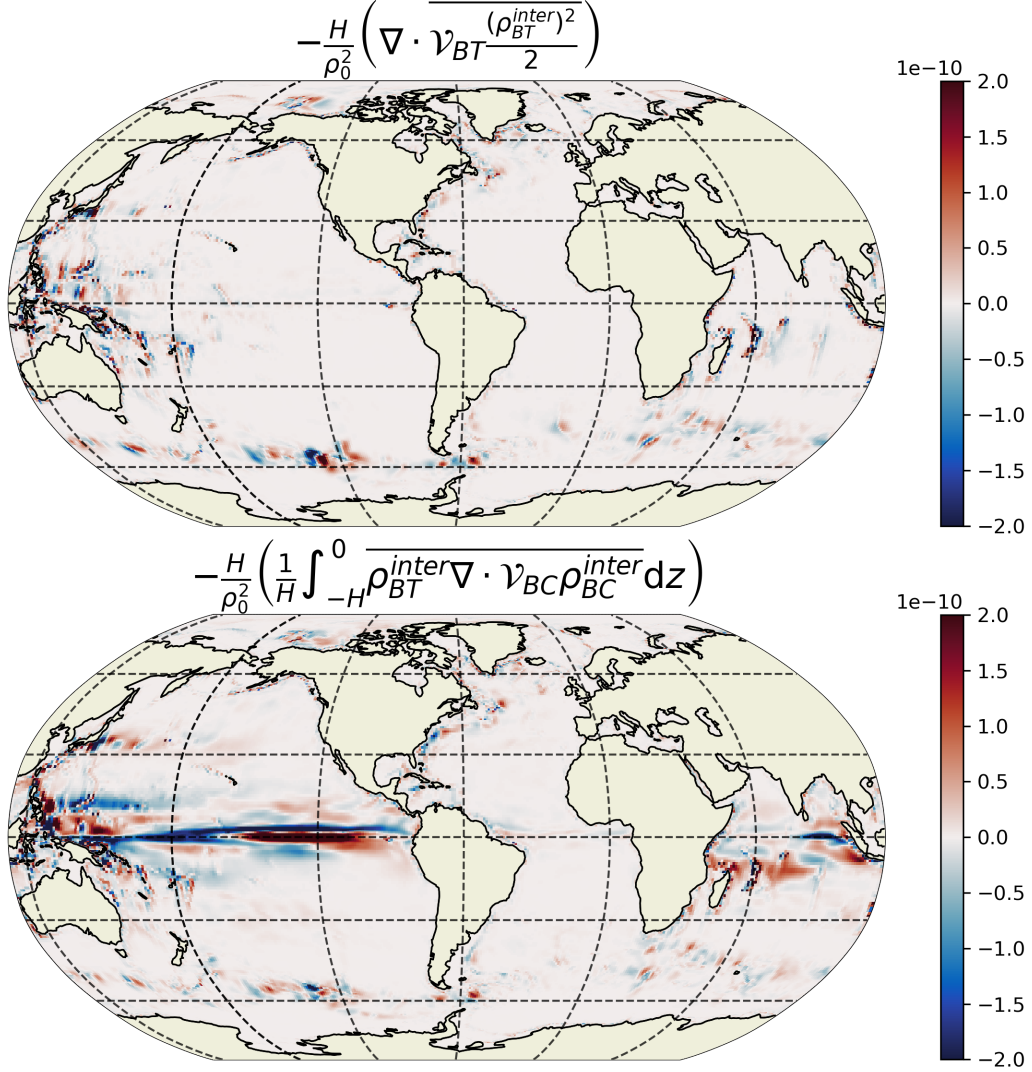


Figure 7. Decomposition of the sum of $\overline{ADV_{steric}^2} + \overline{ADV_{steric}^3}$ (in $m^2 s^{-1}$) as the sum of the convergence of interannual barotropic density variance due to mean and interannual velocities (top panel) and the transfer between the interannual barotropic and baroclinic density variance (bottom panel). The two corresponding formulas in Eq. (31) have been rescaled by H/ρ_0^2 (following Eq. (24)) for easier comparison with the steric sea level terms $\overline{ADV_{steric}^2}$ and $\overline{ADV_{steric}^3}$ from figure 4.

459 This advective source of interannual steric sea level variance is partly compensated
 460 by the term linked with the GM parameterization of eddy induced velocities and by the
 461 resolved subannual oceanic circulation. Resolved subannual frequencies and parametrized
 462 eddies erode the interannual density gradient and thus act as a sink of interannual steric
 463 sea level variability. In this work high frequencies contain every subannual time scales
 464 including the seasonal cycle. It is somehow more traditional in physical oceanography
 465 to sum the seasonal cycle with the mean circulation to create a climatology. However
 466 the non-linear transfer of QG-APE is from low to high frequencies and we thus believe
 467 that it is more physically-sound to use the ordered frequency separation as done in this
 468 work. Preliminary results not shown here further suggest that the energy exchange be-
 469 tween the seasonal cycle and interannual time scales is negligible.

470 Locally in the Equatorial Pacific, the transfer between the vertically integrated in-
 471 terannual barotropic and baroclinic density variance acts as important sink and source
 472 of steric sea level variance. However, when horizontally integrated this term is weakly
 473 negative and thus a global sink of interannual steric sea level variance. It is also inter-
 474 esting to note that, in the Equatorial Pacific, variations of the surface freshwater fluxes
 475 from the atmosphere act as a source of interannual steric sea level variance.

476 An important limitation of this study is the absence of explicit turbulence in the
 477 ECCO V4r3 state estimate due to its laminar resolution and thus to its parametrization
 478 through the GM scheme. We have assumed in this article that the parameterized eddies
 479 are only made of subannual time scales which might not be true everywhere (i.e., per-
 480 manent eddies [or eddies evolving on interannual time scales](#)). Moreover, satellite data
 481 and high-resolution numerical simulations suggest that high levels of steric sea level in-
 482 terannual variability occur in high energetic regions such as in western boundary cur-
 483 rents or in the Antarctic Circumpolar Current (see for instance figure 1 in Carret et al.,
 484 2021). Future work should thus include the effect of a turbulent field in order to (1) avoid
 485 the use of an eddy parameterization that might introduce bias in the results and (2) un-
 486 derstand the mechanisms of steric sea level variance in these eddy-rich regions. Indeed,
 487 [M](#)esoscale eddies are expected to induce an inverse kinetic energy cascade in both space
 488 and time that results in steric sea level variability at interannual time scales (Arbic et
 489 al., 2014; Sérazin et al., 2015). However, the kinetic energy is not the most obvious proxy
 490 for steric sea level variance compared to the APE, for which the cascade is direct (as sug-
 491 gested by the pioneering work on oceanic turbulence of Rhines (1977); Salmon (1978,
 492 1980)). Hence, the HF rectification term by which the HF circulation act as a sink on
 493 interannual steric sea level variability is expected to remain a sink even in the presence
 494 of eddy turbulence, consistently with the present study. The role of the indirect cascade
 495 of kinetic energy for the steric sea level variance budget remains unclear and will there-
 496 fore be the subject of future work. Another potential limitation of this study is the use
 497 of a reanalysis (ECCO V4r3) that adjusts the set of initial conditions, parameters, and
 498 atmospheric boundary conditions to fit observations. The ECCO V4 state estimate, con-
 499 trary to others reanalysis products, obeys the law of physics, but the fitting procedure
 500 might nonetheless induce bias in some of the correlations computed in this article. A per-
 501 spective would thus be to compare our results with that obtained in a forced or free oceanic
 502 run containing eddy turbulence such as DRAKKAR $1/12^\circ$ (Molines et al., 2014) simu-
 503 lations for instance.

504 Finally the steric sea level variance budget appears to be a relatively simple tool
 505 to understand the mechanisms controlling the steric sea level variability. It could thus
 506 be used to help improve the representation of steric sea level variability in different mod-
 507 els, for instance in climate models used for future climate projections, by facilitating the
 508 comparison of the representation of the physical mechanisms at play in these models.

509 **Appendix A HF rectification term in the decomposition of the advective**
 510 **tion**

The high frequency rectification term adv_4 from equation (13) is given by:

$$\text{adv}_4 = -\nabla \cdot (\mathbf{v}^{\text{inter}} \rho^{\text{HF}}) - \nabla \cdot (\mathbf{v}^{\text{HF}} \rho^{\text{inter}}) - \nabla \cdot (\mathbf{v}^{\text{HF}} \rho^{\text{HF}}) + R_{\text{GM}}. \quad (\text{A1})$$

511 where R_{GM} represents the effect of the eddy-induced velocities associated with the GM
 512 parameterization (Gent & McWilliams, 1990).

513 **Appendix B Squared density decomposition**

514 The square of equation (22) is:

$$\begin{aligned} \rho^2 = & \bar{\rho}^2 + (\rho_{\text{BT}}^{\text{inter}})^2 + (\rho_{\text{BC}}^{\text{inter}})^2 + (\rho^{\text{HF}})^2 \\ & + 2\bar{\rho} (\rho_{\text{BT}}^{\text{inter}} + \rho_{\text{BC}}^{\text{inter}} + \rho^{\text{HF}}) \\ & + 2 (\rho_{\text{BT}}^{\text{inter}} \rho_{\text{BC}}^{\text{inter}} + \rho_{\text{BT}}^{\text{inter}} \rho^{\text{HF}} + \rho_{\text{BC}}^{\text{inter}} \rho^{\text{HF}}). \end{aligned} \quad (\text{B1})$$

515 Time averaging gives:

$$\overline{\rho^2} = \bar{\rho}^2 + \overline{(\rho_{\text{BT}}^{\text{inter}})^2} + \overline{(\rho_{\text{BC}}^{\text{inter}})^2} + \overline{(\rho^{\text{HF}})^2} + 2\overline{(\rho_{\text{BT}}^{\text{inter}} \rho_{\text{BC}}^{\text{inter}})}. \quad (\text{B2})$$

516 Then computing the vertical integral gives the decomposition of the vertically integrated
 517 density variance into 4 components:

$$\begin{aligned} \int_{-H}^0 \overline{\rho^2} dz = & \int_{-H}^0 \bar{\rho}^2 dz + \underbrace{\int_{-H}^0 \overline{(\rho_{\text{BT}}^{\text{inter}})^2} dz}_{=H(\rho_{\text{BT}}^{\text{inter}})^2} + \int_{-H}^0 \overline{(\rho_{\text{BC}}^{\text{inter}})^2} dz + \int_{-H}^0 \overline{(\rho^{\text{HF}})^2} dz. \end{aligned} \quad (\text{B3})$$

518 where the fact that $\int_{-H}^0 \rho_{\text{BC}}^{\text{inter}} \rho_{\text{BT}}^{\text{inter}} dz = \rho_{\text{BT}}^{\text{inter}} \int_{-H}^0 \rho_{\text{BC}}^{\text{inter}} dz = 0$, by definition of $\rho_{\text{BC}}^{\text{inter}}$,
 519 and $\int_{-H}^0 \rho_{\text{BT}}^{\text{inter}} dz = H\rho_{\text{BT}}^{\text{inter}}$, by definition of $\rho_{\text{BT}}^{\text{inter}}$, have been used.

520 **Appendix C Decomposition of the advective terms linked with adv_2**
 521 **and adv_3**

522 Inserting adv_2 in Eq. (30) gives:

$$\frac{1}{H} \int_{-H}^0 -\nabla \cdot (\bar{\mathbf{v}} \rho^{\text{inter}}) dz = -\nabla \cdot (\overline{\mathbf{v}_{\text{BT}}} \rho_{\text{BT}}^{\text{inter}}) - \frac{1}{H} \int_{-H}^0 \nabla \cdot (\overline{\mathbf{v}_{\text{BC}}} \rho_{\text{BC}}^{\text{inter}}) dz \quad (\text{C1})$$

523 similarly, inserting adv_3 in Eq. (30) gives:

$$\frac{1}{H} \int_{-H}^0 -\nabla \cdot (\mathbf{v}^{\text{inter}} \rho^{\text{inter}}) dz = -\nabla \cdot (\mathbf{v}_{\text{BT}}^{\text{inter}} \rho_{\text{BT}}^{\text{inter}}) - \frac{1}{H} \int_{-H}^0 \nabla \cdot (\mathbf{v}_{\text{BC}}^{\text{inter}} \rho_{\text{BC}}^{\text{inter}}) dz \quad (\text{C2})$$

524 Then, summing these two equations, multiplying by $\rho_{\text{BT}}^{\text{inter}}$ and time averaging, we recover
 525 equation (31).

526 **Open Research**

527 This study uses the following data: ECCO V4r3 which can be found here: [https://ecco-](https://ecco-group.org/products.htm)
 528 [group.org/products.htm](https://ecco-group.org/products.htm) .

529 **Acknowledgments**

530 ECCO V4r3 salinity and temperature budget computations were greatly facilitated by
 531 the existence of the *ecco-v4-py* Python library, and by several tutorials which can be found
 532 at: <https://ecco-v4-python-tutorial.readthedocs.io/>. We warmly acknowledge the authors
 533 of this work. This work was also supported by the French National Programme LEFE
 534 (Les Enveloppes Fluides de l'Environnement)—GMMC (Groupe Mission Mercator-Coriolis)
 535 by the CRATERE project. [We thank two anonymous reviewers for their valuable com-](#)
 536 [ments and suggestions.](#)

537 **References**

- 538 Arbic, B. K., Müller, M., Richman, J. G., Shriver, J. F., Morten, A. J., Scott, R. B.,
 539 ... Penduff, T. (2014). Geostrophic turbulence in the frequency–wavenumber
 540 domain: Eddy-driven low-frequency variability. *Journal of Physical Oceanogra-*
 541 *phy*, *44*(8), 2050–2069.
- 542 Arzel, O., Huck, T., & Colin de Verdière, A. (2018). The internal generation of
 543 the Atlantic Ocean interdecadal variability. *Journal of Climate*, *31*(16), 6411–
 544 6432.
- 545 Arzel, O., Huck, T., & Colin de Verdière, A. (2006). The different nature of the
 546 interdecadal variability of the thermohaline circulation under mixed and flux
 547 boundary conditions. *Journal of Physical Oceanography*, *36*, 1703–1718.
- 548 Buckley, M. W., Ponte, R. M., Forget, G., & Heimbach, P. (2014). Low-frequency
 549 SST and upper-ocean heat content variability in the North Atlantic. *Journal of*
 550 *Climate*, *27*(13), 4996–5018.
- 551 Carret, A., Llovel, W., Penduff, T., & Molines, J.-M. (2021). Atmospherically
 552 forced and chaotic interannual variability of regional sea level and its com-
 553 ponents over 1993–2015. *Journal of Geophysical Research: Oceans*, *126*(4),
 554 e2020JC017123.
- 555 Cazenave, A., & Llovel, W. (2010). Contemporary sea level rise. *Annual Review of*
 556 *Marine Science*, *2*(1), 145–173.
- 557 Colin de Verdière, A., & Huck, T. (1999). Baroclinic instability: An oceanic wave-
 558 maker for interdecadal variability. *Journal of Physical Oceanography*, *29*(5),
 559 893–910.
- 560 Durand, F., Piecuch, C. G., Becker, M., Papa, F., Raju, S. V., Khan, J. U., &
 561 Ponte, R. M. (2019). Impact of continental freshwater runoff on coastal
 562 sea level. *Surv Geophys*, *40*, 1437–1466. doi: 10.1007/s10712-019-09536-w
- 563 Forget, G., Campin, J.-M., Heimbach, P., Hill, C. N., Ponte, R. M., & Wunsch,
 564 C. (2015). ECCO version 4: An integrated framework for non-linear inverse
 565 modeling and global ocean state estimation [Dataset]. *Geoscientific Model*
 566 *Development*, *8*(10), 3071–3104.
- 567 Fukumori, I., Wang, O., & Fenty, I. (2021). Causal Mechanisms of Sea Level and
 568 Freshwater Content Change in the Beaufort Sea. *Journal of Physical Oceanog-*
 569 *raphy*, *51*(10), 3217–3234. doi: 10.1175/JPO-D-21-0069.1
- 570 Gastineau, G., Mignot, J., Arzel, O., & Huck, T. (2018). North Atlantic Ocean
 571 Internal Decadal Variability: Role of the Mean State and Ocean-Atmosphere
 572 Coupling. *Journal of Geophysical Research: Oceans*, *123*(8), 5949–5970.
- 573 Gent, P. R., & McWilliams, J. C. (1990). Isopycnal mixing in ocean circulation
 574 models. *Journal of Physical Oceanography*, *20*(1), 150–155.
- 575 Gill, A. E., & Niiler, P. P. (1973). The theory of the seasonal variability in the
 576 ocean. *Deep-sea Research*, *20*, 141–177.

- 577 Gregory, J., Griffies, S., & Hughes, C. (2019). Concepts and terminology for sea
578 level: Mean, variability and change, both local and global. *Surv Geophys*, *40*,
579 1251-1289. doi: 10.1007/s10712-019-09525-z
- 580 Hochet, A., Huck, T., Arzel, O., Sévellec, F., & Colin de Verdière, A. (2022). En-
581 ergy transfers between multidecadal and turbulent variability. *Journal of Cli-*
582 *mate*, *35*(4), 1157–1178.
- 583 Hochet, A., Huck, T., Arzel, O., Sévellec, F., Colin de Verdière, A., Mazloff, M., &
584 Cornuelle, B. (2020). Direct temporal cascade of temperature variance in
585 eddy-permitting simulations of multidecadal variability. *Journal of Climate*,
586 *33*(21), 9409–9425.
- 587 Huck, T., Colin de Verdière, A., & Weaver, A. J. (1999). Interdecadal variability
588 of the thermohaline circulation in box-ocean models forced by fixed surface
589 fluxes. *Journal of Physical Oceanography*, *29*(5), 865–892.
- 590 Jackett, D. R., & McDougall, T. J. (1995). Minimal adjustment of hydrographic pro-
591 files to achieve static stability. *Journal of Atmospheric and Oceanic Technol-*
592 *ogy*, *12*(2), 381–389.
- 593 Llovel, W., Fukumori, I., & Meyssignac, B. (2013). Depth-dependent tem-
594 perature change contributions to global mean thermosteric sea level rise
595 from 1960 to 2010. *Global and Planetary Change*, *101*, 113-118. doi:
596 <https://doi.org/10.1016/j.gloplacha.2012.12.011>
- 597 Llovel, W., Guinehut, S., & Cazenave, A. (2010). Regional and interannual vari-
598 ability in sea level over 2002–2009 based on satellite altimetry, Argo float
599 data and GRACE ocean mass. *Ocean Dynamics*, *60*, 1193-1204. doi:
600 10.1007/s10236-010-0324-0
- 601 Llovel, W., & Lee, T. (2015). Importance and origin of halosteric contribution to sea
602 level change in the southeast Indian Ocean during 2005–2013. *Geophysical Re-*
603 *search Letters*, *42*(4), 1148-1157. doi: 10.1002/2014GL062611
- 604 Lombard, A., Cazenave, A., Le Traon, P.-Y., & Ishii, M. (2005). Contribution of
605 thermal expansion to present-day sea-level change revisited. *Global and Plane-*
606 *tary Change*, *47*(1), 1-16. doi: 10.1016/j.gloplacha.2004.11.016
- 607 Meyssignac, B., Piecuch, C. G., Merchant, C. J., Racault, M.-F., Palanisamy, H.,
608 MacIntosh, C., ... Brewin, R. (2017). Causes of the regional variability in
609 observed sea level, sea surface temperature and ocean colour over the period
610 1993–2011. *Surv Geophys*, *38*, 187–215. doi: 10.1007/s10712-016-9383-1
- 611 Molines, J.-M., Barnier, B., Penduff, T., Treguier, A., & Le Sommer, J. (2014).
612 *ORCA12.L46 climatological and interannual simulations forced with*
613 *DFS4.4: GJM02 and MJM88*. (Tech. Rep.). The Drakkar Group: Ex-
614 periment Report GDRI-DRAKKAR-2014-03-19, 50 pp. Retrieved from
615 <https://www.drakkar-ocean.eu/publications/reports/>
- 616 Neumann, B., Vafeidis, A. T., Zimmermann, J., & Nicholls, R. J. (2015, 03). Fu-
617 ture coastal population growth and exposure to sea-level rise and coastal
618 flooding - a global assessment. *PLOS ONE*, *10*, 1-34. doi: 10.1371/
619 journal.pone.0118571
- 620 Nicholls, R. J., & Cazenave, A. (2010). Sea-level rise and its impact on coastal
621 zones. *Science*, *328*(5985), 1517-1520. doi: 10.1126/science.1185782
- 622 Piecuch, C., & Ponte, R. (2011). Mechanisms of interannual steric sea level
623 variability. *Geophysical Research Letters*, *38*(15), L15605. doi: 10.1029/
624 2011GL048440
- 625 Rhines, P. B. (1977). The dynamics of unsteady currents. *The sea*, *6*, 189–318.
- 626 Saji, N., Goswami, B. N., Vinayachandran, P., & Yamagata, T. (1999). A dipole
627 mode in the tropical Indian Ocean. *Nature*, *401*(6751), 360–363.
- 628 Salmon, R. (1978). Two-layer quasi-geostrophic turbulence in a simple special case.
629 *Geophysical & Astrophysical Fluid Dynamics*, *10*(1), 25–52.
- 630 Salmon, R. (1980). Baroclinic instability and geostrophic turbulence. *Geophysical &*
631 *Astrophysical Fluid Dynamics*, *15*(1), 167–211.

- 632 Sérazin, G., Penduff, T., Grégorio, S., Barnier, B., Molines, J.-M., & Terray, L.
633 (2015). Intrinsic variability of sea level from global ocean simulations: Spa-
634 tiotemporal scales. *Journal of Climate*, *28*(10), 4279–4292.
- 635 Sévellec, F., Naveira Garabato, A., & Huck, T. (2021). Damping of climate-scale
636 oceanic variability by mesoscale eddy turbulence. *Journal of Physical Oceanog-
637 raphy*, *51*, 491-503.
- 638 Stammer, D., Cazenave, A., Ponte, R. M., & Tamisiea, M. E. (2013). Causes for
639 contemporary regional sea level changes. *Annual Review of Marine Science*,
640 *5*(1), 21-46. (PMID: 22809188) doi: 10.1146/annurev-marine-121211-172406
- 641 Vallis, G. K. (2017). *Atmospheric and oceanic fluid dynamics*. Cambridge University
642 Press.
- 643 WCRP Global Sea Level Budget Group. (2018). Global sea-level budget 1993–
644 present. *Earth System Science Data*, *10*(3), 1551–1590. doi: 10.5194/essd-10
645 -1551-2018
- 646 Willis, J. K., Roemmich, D., & Cornuelle, B. (2004). Interannual variability
647 in upper ocean heat content, temperature, and thermosteric expansion on
648 global scales. *Journal of Geophysical Research: Oceans*, *109*(C12036). doi:
649 10.1029/2003JC002260